HHS Public Access

Author manuscript

Bone. Author manuscript; available in PMC 2016 December 01.

Published in final edited form as:

Bone. 2015 December ; 81: 620–631. doi:10.1016/j.bone.2015.09.012.

Knee loading protects against osteonecrosis of the femoral head by enhancing vessel remodeling and bone healing

Daquan Liu[a,b,#], **Xinle Li**[a,#], **Jie Li**[a], **Jing Yang**[a], **Hiroki Yokota**[c], and **Ping Zhang**[a,c,*]

[a]Department of Anatomy and Histology, School of Basic Medical Sciences, Tianjin Medical University, Tianjin 300070, China

[b]Department of Pharmacology, Institute of Acute Abdominal Diseases, Tianjin Nankai Hospital, Tianjin 300100, China

[c]Department of Biomedical Engineering, Indiana University-Purdue University Indianapolis, IN 46202, USA

Abstract

Osteonecrosis of the femoral head is a serious orthopedic problem. Moderate loads with knee loading promote bone formation, but its effects on osteonecrosis have not been investigated. Using a rat model, we examined a hypothesis that knee loading enhances vessel remodeling and bone healing through the modulation of the fate of bone marrow-derived cells. In this study, osteonecrosis was induced by transecting the ligamentum teres followed by a tight ligature around the femoral neck. For knee loading, 5 N loads were laterally applied to the knee at 15 Hz for 5 min/day for 5 weeks. Changes in bone mineral density (BMD) and bone mineral content (BMC) of the femur were measured by pDEXA, and ink infusion was performed to evaluate vessel remodeling. Femoral heads were harvested for histomorphometry, and bone marrow-derived cells were isolated to examine osteoclast development and osteoblast differentiation. The results showed that osteonecrosis significant induced bone loss, and knee loading stimulated both vessel remodeling and bone healing. The osteonecrosis group exhibited the lowest trabecular BV/TV ($p < 0.001$) in the femoral head, and lowest femoral BMD and BMC (both $p < 0.01$). However, knee loading increased trabecular BV/TV ($p < 0.05$) as well as BMD and BMC (both $p < 0.05$). Osteonecrosis decreased the vessel volume, vessel number and VEGF expression (all $p < 0.01$), and knee loading increased them (all $p < 0.01$). Osteonecrosis activated osteoclast development, and knee loading reduced its formation, migration, adhesion and the level of “pit” formation (all $p < 0.001$). Furthermore, knee loading significantly increased osteoblast differentiation and CFU-F (both $p < 0.001$). A significant positive correlation was observed between vessel remodeling and bone healing (both $p < 0.01$). These results indicate that knee loading could be effective in repair osteonecrosis of the femoral head in a rat model. This effect might be attributed to promoting vessel remodeling, suppressing osteoclast development, and increasing osteoblast and fibroblast

[*]Corresponding Author: Ping Zhang, MD, Department of Anatomy and Histology, School of Basic Medical Sciences, Tianjin Medical University, 22 Qixiangtai Road, Tianjin 300070, China, Phone: 86-22-83336818, Fax: 86-22-83336810, pizhang2008@163.com.
[#]These authors contributed equally to this work

differentiation. In summary, the current study suggests that knee loading might potentially be employed as a non-invasive therapy for osteonecrosis of the femoral head.

Keywords

Knee loading; Osteonecrosis; Osteoclast; Osteoblast; Vessel remodeling; Bone remodeling

Introduction

Osteonecrosis of the femoral head (ONFH) is a disease in which bone death occurs as a result of impairment of blood supply to the femoral head [1, 2]. There are several etiologic risk factors such as trauma [3, 4], excessive corticosteroid use [5–7], excessive alcohol intake [8], Legg-Calve-Perthes disease [9, 10], etc. Debilitated blood supply to the femoral head commonly leads to necrosis and collapse of the femoral head [11]. In spite of various research efforts and trials, ONFH is still one of the most serious orthopedic problems. More than 500,000 hip replacements were performed for ONFH patients annually in the United States, and 10% of them required surgical debridement of dead bone [12]. Many therapies have been applied to animal models and patients to prevent the progress of ONFH. Non-surgical therapies include anti-osteoporosis medicine, anticoagulants, decreasing weight bearing, lipid-lowering medicine, electromagnetic stimulation, shockwave therapy and hyperbaric oxygen therapy, while surgical therapies consist of autologous bone marrow stem cell transplantation, core decompression and total hip replacement [13, 14]. Most of these therapies, however, have limits and side-effects. It is thus important and urgent to develop safe and effective treatment for ONFH.

Joint loading is one form of non-invasive physical treatment. Joint loading have been applied to synovial joints such as the elbow, knee and ankle [15]. In our previous studies, joint loading were applied 3 to 5 min per day for 2 to 3 weeks. Our bone histomorphometric studies demonstrated that knee loading stimulates bone formation [16]. We have also demonstrated that knee loading can accelerate the healing of surgical wounds in the femoral neck and tibia [15, 17].

The mechanism of knee loading is considered to change intramedullary pressure of femoral and tibial bone cavities. The load-driven pressure may generate fluid flow in a lacuna canalicular network in bone cortex. The pressure also activates bone metabolism-related genes in femur and tibia [18, 19]. In our previous works, knee loading stimulated bone formation by conducting bone histomorphometry using the cross-sections at 25% (distal femur), 50% (midshaft), and 75% (proximal femur) of the length of the femur from the loading site. Knee loading also induced bone formation and enhanced bone healing in the femoral neck [20]. In this study, we addressed a question whether knee loading improves experimentally induced ONFH by modulating both vessel remodeling and bone remodeling. Our hypothesis was that knee loading would enhance vessel remodeling and bone healing through the modulation of the fate of bone marrow-derived cells.

To test the hypothesis, a rat model of ONFH was induced by transecting the ligamentum teres followed by a tight ligature around the femoral neck. The knee joint received loading

for 5 wks. We evaluated the effects of knee loading focusing on BMD and BMC using pDEXA. Ink infusion and histology assay were performed to evaluate vessel remodeling and bone healing. We also evaluated the effects of knee loading on the functions of osteoblast and osteoclast of bone marrow-derived cells.

Materials and Methods

Animals and materials preparation

Male Sprague-Dawley rats (~12 weeks of age, Animal Center of Academy of Military Medical Sciences, China) were used. The rats were housed on a 12:12 h light-dark cycle under pathogen-free conditions and were feed with food and water *ad libitum*. All experiments were carried out according to the National Institutes of Health Guide for Care and Use of Laboratory Animals and were approved by the Ethics Committee of Tianjin Medical University. Murine receptor activator of nuclear factor kappa-B ligand (RANKL) and murine macrophage-colony stimulating factor (M-CSF) were purchased from PeproTech (Rocky Hills, NC, USA). VEGF polyclonal antibody was purchased from Proteintech (Chicago, IL, USA). Immunohistochemical staining kit and 3, 3′-diaminobenzidine (DAB) substrate kit were purchased from ZSGB-BIO (Beijing, China). Dulbecco's Modi ed Eagle's Medium (DMEM), Minimum Essential Medium Alpha (MEM-α), fetal bovine serum, penicillin, streptomycin and trypsin were purchased from Invitrogen (Carlsbad, CA, USA). Other chemicals were purchased from Sigma (St. Louis, MO, USA).

Experimental design

Eighteen rats were randomly divided into 3 groups: sham operated control group (Sham), osteonecrosis group (ON), and knee loading treated osteonecrosis group (ON+Loading) (n = 6). Ischemic osteonecrosis of the bilateral femoral heads were induced using the previously described method with minor modifications [3].

Surgical procedure to induce osteonecrosis

The rat was placed in an anesthetic induction chamber to cause sedation and then mask-anesthetized using 2% isoflurane (IsoFlo, Abbott Laboratories, North Chicago, IL, USA) at a flow rate of 1.0 to 1.5 L/min. A longitudinal incision was made on the skin over the large trochanter. The gluteus maximus muscle and the gluteus medius muscle were separated from the bone. The joint capsule of hip was transected and the femoral head was dislocated (Fig. 1A). Osteonecrosis of the femoral head was induced by transecting the ligamentum teres and tightly placing a ligature (#3-0 Vicryl, Ethicon) around the femoral neck (Fig. 1B). The femoral head was relocated, and gluteal muscles and skin were sutured with #3-0 and #4-0 stitches, respectively. Osteonecrosis was induced on both left and right side. For sham operation, a joint capsule was not transected and a femoral neck received no ligation. In order to alleviate the pain associated with surgery, analgesia was conducted. The rat was given a dose of buprinorphine hydrochloride (0.05 mg/kg) at rate of 0.2 ml subcutaneously before incision. 1% pramoxine hydrochloride ointment was applied on the incision sites after surgery. Buprinorphine hydrochloride (0.05 mg/kg) was also administered per 8 hr for the first three postoperative days, and applied until a week if necessary. In addition,

antibiotic prophylaxis (enrofloxacin, 5 mg/kg) was administered per day for the first three postoperative days.

Knee loading

The joint loading equipment in the form of knee, ankle, and elbow loading is a recently devised treatment modality (Fig. 1 C) [21]. In this current study, knee loading was achieved through dynamic loads applied to the left and right knee joint of rats in the lateral-medial direction, respectively. To position the knee properly, the lower end of the loading rod and the upper end of the stator were designed to form a pair of semispherical cups. The lateral and medial epicondyles of the femur together with the lateral and medial condyles of the tibia were confined in the cups (Fig. 1 D) [22]. The tip of the loader had a contact area of 15 mm in diameter. Knee loading was conducted one week after operation. Anesthesia was induced with 2% isoflurane at a flow rate of 1.0 to 1.5 L/min. With the custom-made loader, knee loading (5 N force) was laterally applied to the left and right knee successively at 15 Hz for 5 min/day for 5 weeks. Animals were sacrificed 5 weeks after loading. Femurs and tibias were collected, and bone marrow cells were isolated.

Measurements of bone mineral density (BMD) and bone mineral content (BMC)

The animals were anesthetized by 2% isoflurane at a flow rate of 1.0 to 1.5 L/min, placed on the platform in the prone position, and images were acquired in about 5 min. Bone mineral density (BMD, g/cm^2) and bone mineral content (BMC, g) of the femur were measured by peripheral dual-energy X-ray absorptiometry (pDEXA) before surgery and sacrifice. Changes in BMD and BMC were determined and statistical analysis was conducted.

Vessel remodeling assay

To evaluate vessel remodeling of the femoral head, a blood circulation assay was performed. Chinese ink was infused 6 weeks after the operation using the procedure with minor modification [23]. The animals were anesthetized by an intraperitoneal injection of 10% chloral hydrate (3 ml/kg). The chest was opened and the heart was exposed. A needle was inserted into the left ventricle for ink infusion, and the right atrium was cut. Animals were flushed with a heparin-saline solution (25,000 units in 250 ml of 0.9% sodium chloride) until clear liquid flowed from the circulation. The 5% gelatin/ink solution (the ratio between Chinese ink and water was 1:1) was injected into the circulation until the skin of animals became uniformly black. After euthanizing the animals, a pair of femoral heads was harvested.

Histology and immunohistochemistry assay

After sacrifice, bilateral femoral heads were harvested and fixed in 10% neutral buffered formalin for 2 days. Samples were decalcified in 10% ethylenediaminetetraacetic acid (EDTA, pH 7.4) for 40 days and embedded in paraffin. The samples were cut with a Leica RM2255 microtome (Leica Microsystems Inc., Bannockburn, IL) into 5-μm thick slices along the coronal plane. Sections were stained with hematoxylin-eosin (H&E) for examining osteonecrosis and histological parameters. The images of the femoral head were captured with an Olympus BX53 microscope and Olympus DP73 camera. Measurement of bone mass

was performed within the trabecular area on the femoral head, in which bone volume fraction BV/TV (in %, TV, total tissue area, calculated from the total tissue area; and BV, trabecular bone area, calculated from the total trabecular area) was determined [24–27]. Furthermore, we used tartrate resistant acid phosphatase (TRAP) staining to determine osteoclast activity according to the standard protocol (Sigma). The ratio between length of TRAP-positive cells and total circumference of bone trabecula was calculated. It represented the activity of osteoclast. As described previously, MacNeal's staining was used for identifying osteoblasts [28, 29]. The quantification of osteoblast cells number was normalized to the bone trabecular surface in each histological section. Immunohistochemical staining was performed using immunohistochemical kit and 3, 3′-diaminobenzidine (DAB) substrate kit according to the protocol of manufacturer. The sections were incubated with the primary antibody of VEGF (1:50) overnight at 4°C. The ratio of VEGF positively stained area to total field area was calculated [23, 30]. For ink infusion, the samples were cut into 25-μm thick slices. The vessel number per field and the ratio of vessel volume to total field area were calculated, respectively. For all histological assays, five fields per slice (100–400×) were randomly selected, and the structural and vascular parameters were determined using Cellsense Standard software (Olympus).

Bone marrow-derived cells culture and osteoblast/osteoclast differentiation

The method to collect bone marrow-derived cells was described previously [31]. The tibias were flushed with DMEM containing 2% fetal bovine serum (FBS). The cells were separated using Ficoll low-density gradient centrifugation. For osteoclast differentiation, cells were cultured in MEM-α with 10% FBS, 30 ng/ml M-CSF and 20 ng/ml RANKL. For osteoblast differentiation, cells were cultured in osteogenic differentiation medium (MesenCult proliferation kit) with supplemented reagent. All cell cultures were maintained at 37°C in a humidified atmosphere of 5% CO_2.

Colony-forming unit-granulocyte-macrophages (CFU-GM) and Colony-forming unit-macrophage/mononuclear (CFU-M) assay

CFU-GM and CFU-M assay were conducted using the procedure described previously [31, 32]. Bone marrow-derived cells were seeded onto 6-well plates at a density of 2.5×10^4 cells/well. The culture medium was composed of methylcellulose with 30 ng/ml M-CSF and 20 ng/ml RANKL. Cells were cultured at 37°C in a 5% CO_2 incubator for 7 days. The number of colonies was counted in each well using phase-contrast microscopy. The colony numbers of CFU-M were converted to the numbers per tibia.

Osteoclast formation assay

Bone marrow-derived cells were seeded onto 96-well plates at a density of 1×10^5 cells/well, and cultured in MEM-α supplemented 10% FBS, 30 ng/ml M-CSF, and 20 ng/ml RANKL for two days [33]. On the third day, the culture medium was replaced by MEM-α supplemented with 10% FBS, 30 ng/ml M-CSF, and 60 ng/ml RANKL, and cells were grown for an additional 3 days. We used a tartrate resistant acid phosphate (TRAP) staining kit (Sigma) and determined osteoclast formation on day 6 according to the manufacturer's protocol. TRAP-positive multinuclear cells (more than 3 nuclei) were identified as

osteoclasts. Five fields per well (400×) were randomly selected, and the ratio of the osteoclast area to the total field area was determined using Cellsense standard software.

Osteoclast migration assay

Migration of osteoclasts was evaluated using a transwell assay as described previously with minor modifications [31]. Bone marrow-derived cells (2×10^6 cells/ml in 6-well plates) were cultured in MEM-α supplemented 10% FBS, 30 ng/ml M-CSF and 20 ng/ml RANKL for 4 days. The osteoclast precursor cells (1×10^5 cells/well) were loaded onto the upper chamber of transwells and allowed to migrate to the bottom chamber through an 8-μm polycarbonate filter coated with vitronectin (Takara Bio Inc., Otsu, Shigma, Japan). The medium in the upper chamber was replaced with free serum MEM-α, and the lower chamber contained MEM-α consisting of 1% bovine serum albumin (BSA) and 30 ng/ml M-CSF. After 6 h reaction, cells were stained with crystal violet, and the number of osteoclast precursor cells in the lower chamber (attached onto the bottom of the transwells) was counted. Five fields per well (200×) were randomly selected and photographed for counting.

Osteoclast adhesion assay

Bone marrow-derived cells were cultured in MEM-α supplemented 10% FBS, 30 ng/ml M-CSF and 20 ng/ml RANKL for 4 days. Then osteoclast precursor cells were plated onto 96-well plates coated with vitronectin at a density of 1×10^5 cells/well in MEM-α supplemented with 30 ng/ml M-CSF. After 30 min of incubation, cells were washed with PBS three times and fixed with 4% paraformaldehyde at room temperature for 10–15 min. Adherent cells were stained with crystal violet. Five fields per well (200×) were randomly selected, and the number of cells adherent to the bottom of plates was counted [34].

Pit formation assay

To determine bone resorption ability of bone marrow-derived cells, a pit formation assay was performed according to the previously described method with minor modifications [33]. UV-sterilized bovine cortical bone slices (120 μm thick) were placed in a bottom of a 24-well plate. Bone marrow-derived cells were seeded onto the plate at a density of 1×10^5 cells/well, and cultured for two days in MEM-α supplemented 10% FBS, 30 ng/ml M-CSF, and 20 ng/ml RANKL. On the third day, the concentration of RANKL was increased to 60 ng/ml, and the medium was changed every 2 days. The bone slices were stained with crystal violet on day 10. Five fields per well (400×) were randomly selected, and the ratio of the pit area to the total field area was determined.

Osteoblast differentiation assay

For osteoblast differentiation, 2×10^6 cells/ml bone marrow-derived cells were seeded onto 6-well plates with osteogenic differentiation medium (MesenCult proliferation kit, supplemented with 10 nM dexamethasone, 50 μg/ml ascorbic acid 2-phosphate, and 10 mM β-glycerophosphate). The medium was changed every 2 days, and cells were cultured for 14 days. ALP staining kit (Sigma) was used for alkaline phosphatase (ALP) staining. Cells were fixed in citrate-buffered acetone for 30 s, incubated in the alkaline-dye mix for 30 min, and counterstained with Mayer's Hematoxylin for 10 min. Five fields (400×) per well were

randomly selected, and the ratio of the number of ALP-positive cells to that of the total cells was determined microscopically.

Colony-forming unit- fibroblast (CFU-F) assay

To evaluate the ability of fibroblast-like mesenchymal stem cell (MSC) colony formation in the CFU-F assay, 2×10^6 cells/ml bone marrow-derived cells were seeded onto 6-well plates with complete MesenCult medium. Fresh medium was exchanged every other day, and cells were cultured for 14 days. On day 14, cells were rinsed with PBS and stained using a HEMA-3 quick staining kit (Fisher Scientific, Waltham, MA, USA). The number of colonies with more than 50 cells was counted in each well, and the clusters of cells that did not present fibroblast-like morphology were excluded.

Statistical analysis

Data were expressed as mean ± standard error of mean (SEM). Data were analyzed with one-way analysis of variance (one-way ANOVA) and a post hoc test of least signicant difference (LSD). Correlation analysis of parameters was performed by using Pearson correlation coefficient test. Statistical significance was assumed at $p < 0.05$. The asterisks (*, **and ***) represent $p < 0.05$, $p < 0.01$ and $p < 0.001$, respectively.

Results

No infections were detected at the surgical site during the 6-week course of experiments. We did not observe any abnormal behavior, weight loss, or diminished food intake.

Knee loading enhanced femoral BMD/BMC of the osteonecrosis rats

To determine any change in bone in the osteonecrosis and knee loading groups, BMD and BMC were measured before surgery and sacrifice. During the 6-week period, the osteonecrosis group showed the lowest increase in femoral BMD and BMC (both $p < 0.01$) (Fig. 1E, F). However, knee loading significantly increased femoral BMD ($p<0.05$) and BMC ($p < 0.01$) (Fig. 1E, F).

Knee loading improved ischemic femoral head

To examine whether knee loading improves ischemic femoral heads, we determined the geometric parameters of femoral heads. The femoral head surface of the sham operated control was smooth, while that of the osteonecrosis group exhibited “moth eaten” appearance (indicated by the arrows). The surface of femoral head of the loading group presented between the two other groups (Fig. 2A). Geometric inspection revealed that compared to the sham operated control, the samples in the osteonecrosis group exhibited shorter height of the femoral head. Knee loading improved the height of the femoral head, although the increase approached statistical significance (data not shown).

In the sections stained with H&E (Fig. 2B), the osteonecrosis group exhibited a lower ratio of the trabecular volume to the tissue volume (BV/TV) ($p < 0.001$). Compared to the osteonecrosis group, knee loading increased BV/TV of the femoral head ($p < 0.05$; Fig. 2C).

Knee loading enhanced vessel remodeling

To determine whether knee loading enhances vessel remodeling in the ischemic femoral head, we determined the expression of VEGF which immunoreactivity was mainly observed in endothelial cells. Several VEGF positive staining microvessels were found in sham and loading groups. However, it was seldom seen in osteonecrosis group (Fig. 3A). The ratio of VEGF positively stained area to total field area was calculated. Osteonecrosis decreased the expression of VEGF ($p < 0.01$), and knee loading significantly enhanced them ($p < 0.01$; Fig. 3B). We also analyzed microvessels using blood perfusion angiography (Fig. 3C). Osteonecrosis decreased both the vessel volume and the vessel number (both $p < 0.001$), and knee loading enhanced them (both $p < 0.001$; Fig. 3D, E).

Knee loading reduced the numbers of CFU-GM and CFU-M

To determine whether knee loading affected the proliferation of osteoclast progenitors, the CFU-GM and CFU-M assays were conducted. The numbers of CFU-GM and CFU-M per tibia were increased in the osteonecrosis group (both $p < 0.001$). However, the numbers of CFU-GM (Fig. 4A) and CFU-M (Fig. 4B) were significantly reduced by knee loading (both $p < 0.001$).

Knee loading suppressed osteoclast formation

To determine whether knee loading affected the formation of osteoclasts *in vitro*, bone marrow-derived cells were treated with M-CSF and RANKL. Compared to the sham group, cells from the osteonecrosis group exhibited a signicantly increased capacity to form matured osteoclasts (Fig. 4C). The loading group, however, presented significantly lowered matured osteoclasts ($p < 0.001$; Fig. 4D).

Knee loading suppressed migration and adhesion of pre-osteoclasts

To evaluate whether knee loading simultaneously suppressed migration and adhesion, we conducted assays for migration (Fig. 5A) and adhesion (Fig. 5B). The osteonecrosis group elevated both migration and adhesion (both $p < 0.001$), while knee loading signicantly attenuated both migration ($p < 0.01$; Fig. 5C) and adhesion ($p < 0.001$; Fig. 5D).

Knee loading suppressed bone resorption of osteoclasts

For the histological samples, TRAP staining showed that the ratio of TRAP-positive cells was increased in the osteonecrosis group ($p < 0.01$; Fig. 6A), and the elevated ratio in the osteonecrosis group was significantly suppressed by knee loading ($p < 0.05$; Fig. 6B).

The ratio of the pit area to the total field area was calculated (Fig. 6C). Cells from the osteonecrosis group exhibited an increased capacity to form pits. Compared to the osteonecrosis group, pit formation was signicantly suppressed by knee loading ($p < 0.001$; Fig. 6D).

Knee loading enhanced osteoblast differentiation in vivo and in vitro

We next determined whether knee loading had an effect on the differentiation of osteoblasts *in vivo* and *in vitro*. For the histological samples, MacNeal's staining was used to identify

osteoblasts in the femoral head (Fig. 7A). The data showed that the number of osteoblasts was not significantly different in the sham and osteonecrosis groups. However, it signicantly increased in the loading group ($p < 0.01$; Fig. 7 B). For bone marrow-derived cells, the percentage of ALP-positive cells in total cells was not significantly different between the sham and osteonecrosis groups. However, the loading significantly increased the percentage of ALP-positive cells ($p < 0.001$; Fig. 7C, D).

Knee loading increased the number of CFU-F

To evaluate any effect of knee loading on the differentiation from marrow mesenchymal progenitors to fibroblasts, we performed the CFU-F assay 14 days after isolation of bone marrow-derived cells (Fig. 7E). The result revealed that the loading group generated a significantly higher number of CFU-F than the sham and osteonecrosis groups ($p < 0.001$; Fig. 7F).

The correlation analysis between the parameters of vessel remolding and bone healing

To evaluate whether vessel remolding was correlated with bone remolding, we selected parameters of vessel remodeling (vessel volume and vessel number) and bone remolding (BMD, BMC and BV/TV) to analyze the correlation. The statistic analysis indicated that vessel volume were positively corrected with BMD, BMC and BV/TV (r = 0.891, 0.898 and 0.920, respectively, all $p < 0.01$). We also observed that vessel number were positively corrected with BMD, BMC and BV/TV (r = 0.901, 0.918 and 0.924, respectively, all $p < 0.01$) (Fig. 8).

Discussion

ONFH is one of the serious orthopedic diseases in the hip joint [35]. Many therapies have been applied to animal models of ONFH to investigate the curative effect. Therefore, establishing a suitable animal model is indispensable to improve the diagnosis and therapy. Although various risk factors are considered [36], interruption of blood supply to the femoral head is a core factor [37]. So, the pathogenesis of animal models of ONFH is corrected with interruption of blood supply in femoral head directly and indirectly. There are multiple animal models such as spontaneous osteonecrosis, surgical-induced osteonecrosis, corticosteroid-induced osteonecrosis, endotoxin-induced osteonecrosis, and physical injury-induced osteonecrosis [38]. Spontaneous osteonecrosis, for instance, induces osteonecrosis by compressing arteries that enter the femoral head [39]. In surgical-induced osteonecrosis, two major procedures are ligation of the femoral neck and cutting the ligamentum teres. Excessive corticosteroids intake is a risk factor, since concentrated corticosteroids can block microvessels by forming fat embolism [6, 23]. ONFH can also be induced by lipopolysaccharide alone or lipopolysaccharide combined with corticosteroids. Rabbits usually are sensitive to lipopolysaccharide, and its intravenous injection may lead to multifocal osteonecrosis in the femoral head [40]. Physical injury, such as exposure to low temperature with liquid nitrogen, may induce ONFH by promoting thrombosis in microvessels [41].

An ischemic osteonecrosis model of Yorkshire pigs was employed by transecting the ligamentum teres and placing two ligatures around the femoral neck [42]. Using optical and CT imaging analysis, we demonstrated that the ligatures around the femoral neck were the primary cause of induction of avascular osteonecrosis. In our study, ONFH was induced by transecting the ligamentum teres and tightly placing a ligature around the femoral neck in a rat model for six weeks. Anatomical inspection revealed that compared to the sham operated control, the femoral head of the osteonecrosis group exhibited non-smooth and somewhat greater “moth eaten” appearance. The samples in the osteonecrosis group exhibited shorter height of the femoral head. Histological observation revealed that compared to the sham group, the osteonecrosis group exhibited the smaller BV/TV, vessel volume and vessel number. We also observed that ONFH stimulated maturation, migration, adhesion, and pit formation (bone resorption) of osteoclasts. In many skeletal diseases including osteoporosis, osteoarthritis and osteonecrosis, osteoclast activities increase [43–45], and our results accord with them. Furthermore, geometric inspection revealed that the samples in the osteonecrosis group exhibited a shorter height and width of the femoral head than the sham operated control group. Collectively, the animal model herein is a proper experimental model for mimicking an avascular osteonecrosis.

Knee loading presented multiple beneficial effects on vessel remodeling and bone remodeling. In bone remodeling, we observed that knee loading increased femoral BMD/BMC and BV/TV. Knee loading increased the height of the femoral head partially, although the increase approached statistical significance potentially because of a relatively short period to observation. In vessel remodeling, data in the blood perfusion assay indicated that knee loading suppressed the ONFH-induced decrease in the vessel volume and vessel number. We also determined the expression of VEGF (an essential angiogenic marker). Knee loading increased the expression of VEGF and the VEGF positive staining microvessels in femoral head of ONFH. It indicated that knee loading improved vessel remodeling by increasing both blood perfusion and angiogensis in ONFH. Our previous paper indicated that collateral circulation around the femoral neck was altered in a pig osteonecrosis model [42]. We would determine the effect of knee loading to collateral circulation around the femoral head in the further study. In bone homeostasis, balance between bone formation by osteoblasts and bone resorption by osteoclasts is required [46]. We conducted *in vitro* assays and evaluated the role of knee loading in the fate of bone marrow-derived cells. On one hand, our data indicated that knee loading suppressed maturation, migration, adhesion, and pit formation (bone resorption) of osteoclasts. On the other hand, we observed that differentiation of osteoblasts and fibroblasts was not affected in ONFH. However, knee loading enhanced differentiation of osteoblasts and fibroblasts. In addition, we used static bone histomorphometry to determine osteoblast (MacNeal’s staining) and osteoclast (TRAP staining) numbers in the femur. The data indicated that knee loading stimulated differentiation of osteoblasts and suppressed activity of osteoclasts *in vivo*. The results support the notion that knee loading achieves not only suppression of bone loss but also stimulation of bone formation. The results of correlation analysis indicated that a significant positive correlation was observed between vessel remodeling (vessel volume and vessel number) and bone remolding (BMD, BMC and BV/TV). Many factors can contribute to the observed bone healing including load-induced blood perfusion, a decrease

in bone-resorbing osteoclasts and an increase in bone-forming osteoblasts. The current histology and bone mineral density data are suggestive of the role of bone marrow-derived stem cells in load-driven bone healing, and they also establish a causal relationship between the observed vessel remodeling and bone healing effects with knee loading (Fig. 8).

Loading synovial joints such as the knee and ankle has been demonstrated to accelerate the healing of surgical wounds in the femoral neck and tibia, respectively [15, 17]. Joint loading is also reported to elevate the length of mouse limbs [47, 48]. Our previous microarray analysis using C57BL/6 female mice indicated that signaling pathways related to Wnt, PI3K, TGF-β and ECM-receptors are involved in the responses to joint loading [18]. Answering to a question whether these pathways mediate the observed bone remodeling as well as vessel remodeling requires further molecular analysis.

In conclusion, we demonstrate that knee loading is effective in improving ONFH in a rat model. Knee loading achieve bone healing through promoting both vessel remodeling and bone remodeling in the femur through the modulation of the fate of bone marrow-derived cells in the treatment of ONFH. Further studies should be performed to clarify the molecular mechanism underlying the role of bone marrow-derived cells in vessel remodeling as well as bone remodeling. The present study suggests that knee loading has a potential usage as a non-invasive physical therapy for ONFH.

Acknowledgments

This study was supported by grant (81572100 to PZ) from the National Natural Science Foundation of China, grant (14JCZDJC36500 to PZ) from the Tianjin Municipal Science and Technology Commission and NIH AR052144 (to HY).

Abbreviations

ONFH	Osteonecrosis of the femoral head
RANKL	Receptor activator of nuclear factor kappa-B ligand
M-CSF	Macrophage-colony stimulating factor
BMD	Bone mineral density
BMC	Bone mineral content
TRAP	Tartrate resistant acid phosphatase
ALP	Alkaline phosphatase

References

1. Feng Y, Yang SH, Xiao BJ, Xu WH, Ye SN, Xia T, Zheng D, Liu XZ, Liao YF. Decreased in the number and function of circulation endothelial progenitor cells in patients with avascular necrosis of the femoral head. Bone. 2010; 46:32–40. [PubMed: 19747991]
2. Kamiya N, Yamaguchi R, Aruwajoye O, Adapala NS, Kim HK. Development of a mouse model of ischemic osteonecrosis. Clin Orthop Relat Res. 2015; 473:1486–98. [PubMed: 25666143]
3. Little DG, Peat RA, McEvoy A, Williams PR, Smith EJ, Baldock PA. Zoledronic acid treatment results in retention of femoral head structure after traumatic osteonecrosis in young Wistar rats. J Bone Miner Res. 2003; 18:2016–22. [PubMed: 14606515]

4. Aruwajoye OO, Patel MK, Allen MR, Burr DB, Aswath PB, Kim HK. Microcrack density and nanomechanical properties in the subchondral region of the immature piglet femoral head following ischemic osteonecrosis. Bone. 2013; 52:632–9. [PubMed: 22889721]
5. Yoshioka T, Mishima H, Akaogi H, Sakai S, Li M, Ochiai N. Concentrated autologous bone marrow aspirate transplantation treatment for corticosteroid-induced osteonecrosis of the femoral head in systemic lupus erythematosus. Int Orthop. 2011; 35:823–9. [PubMed: 20512330]
6. Zaidi M, Sun L, Robinson LJ, Tourkova IL, Liu L, Wang Y, Zhu LL, Liu X, Li J, Peng Y, Yang G, Shi X, Levine A, Iqbal J, Yaroslavskiy BB, Isales C, Blair HC. ACTH protects against glucocorticoid-induced osteonecrosis of bone. Proc Natl Acad Sci U S A. 2010; 107:8782–7. [PubMed: 20421485]
7. Tian L, Wen Q, Dang X, You W, Fan L, Wang K. Immune response associated with Toll-like receptor 4 signaling pathway leads to steroid-induced femoral head osteonecrosis. BMC Musculoskelet Disord. 2014; 15:18. [PubMed: 24428851]
8. Wang C, Wang J, Zhang Y, Yuan C, Liu D, Pei Y, Li X, Wu Z, Li Y, Guo Z. A canine model of femoral head osteonecrosis induced by an ethanol injection navigated by a novel template. Int J Med Sci. 2013; 10:1451–8. [PubMed: 24046517]
9. Kamiya N, Yamaguchi R, Adapala NS, Chen E, Neal D, Jack O, Thoveson A, Gudmundsson P, Brabham C, Aruwajoye O, Drissi H, Kim HK. Legg-calve-perthes disease produces chronic hip synovitis and elevation of interleukin-6 in the synovial fluid. J Bone Miner Res. 2015; 30:1009–13. [PubMed: 25556551]
10. Hyman JE, Trupia EP, Wright ML, Matsumoto H, Jo CH, Mulpuri K, Joseph B, Kim HK. International Perthes Study Group M. Interobserver and intraobserver reliability of the modified Waldenstrom classification system for staging of Legg-Calve-Perthes disease. J Bone Joint Surg Am. 2015; 97:643–50. [PubMed: 25878308]
11. Hang D, Wang Q, Guo C, Chen Z, Yan Z. Treatment of osteonecrosis of the femoral head with VEGF165 transgenic bone marrow mesenchymal stem cells in mongrel dogs. Cells Tissues Organs. 2012; 195:495–506. [PubMed: 22056983]
12. Mankin HJ. Nontraumatic necrosis of bone (osteonecrosis). N Engl J Med. 1992; 326:1473–9. [PubMed: 1574093]
13. Castro FP Jr, Barrack RL. Core decompression and conservative treatment for avascular necrosis of the femoral head: a meta-analysis. Am J Orthop (Belle Mead NJ). 2000; 29:187–94. [PubMed: 10746469]
14. Ajmal M, Matas AJ, Kuskowski M, Cheng EY. Does statin usage reduce the risk of corticosteroid-related osteonecrosis in renal transplant population? Orthop Clin North Am. 2009; 40:235–9. [PubMed: 19358908]
15. Zhang P, Yokota H. Knee loading stimulates healing of mouse bone wounds in a femur neck. Bone. 2011; 49:867–72. [PubMed: 21723427]
16. Zhang P, Tanaka SM, Jiang H, Su M, Yokota H. Diaphyseal bone formation in murine tibiae in response to knee loading. J Appl Physiol (1985). 2006; 100:1452–9. [PubMed: 16410382]
17. Zhang P, Sun Q, Turner CH, Yokota H. Knee loading accelerates bone healing in mice. J Bone Miner Res. 2007; 22:1979–87. [PubMed: 17696761]
18. Zhang P, Turner CH, Yokota H. Joint loading-driven bone formation and signaling pathways predicted from genome-wide expression profiles. Bone. 2009; 44:989–98. [PubMed: 19442616]
19. Zhang P, Su M, Liu Y, Hsu A, Yokota H. Knee loading dynamically alters intramedullary pressure in mouse femora. Bone. 2007; 40:538–43. [PubMed: 17070127]
20. Zhang P, Tanaka SM, Sun Q, Turner CH, Yokota H. Frequency-dependent enhancement of bone formation in murine tibiae and femora with knee loading. J Bone Miner Metab. 2007; 25:383–91. [PubMed: 17968490]
21. Zhang P, Hamamura K, Yokota H, Malacinski GM. Potential applications of pulsating joint loading in sports medicine. Exerc Sport Sci Rev. 2009; 37:52–6. [PubMed: 19098525]
22. Zhang P, Su M, Tanaka SM, Yokota H. Knee loading stimulates cortical bone formation in murine femurs. BMC Musculoskelet Disord. 2006; 7:73. [PubMed: 16984642]

23. Fan L, Li J, Yu Z, Dang X, Wang K. Hypoxia-inducible factor prolyl hydroxylase inhibitor prevents steroid-associated osteonecrosis of the femoral head in rabbits by promoting angiogenesis and inhibiting apoptosis. PLoS One. 2014; 9:e107774. [PubMed: 25244080]
24. Byers S, Moore AJ, Byard RW, Fazzalari NL. Quantitative histomorphometric analysis of the human growth plate from birth to adolescence. Bone. 2000; 27:495–501. [PubMed: 11033444]
25. Xian CJ, Cool JC, Scherer MA, Macsai CE, Fan C, Covino M, Foster BK. Cellular mechanisms for methotrexate chemotherapy-induced bone growth defects. Bone. 2007; 41:842–50. [PubMed: 17884747]
26. Lee AM, Morrison JL, Botting KJ, Shandala T, Xian CJ. Effects of Maternal Hypoxia during Pregnancy on Bone Development in Offspring: A Guinea Pig Model. Int J Endocrinol. 2014; 2014:916918. [PubMed: 24949010]
27. Xian CJ, Cool JC, Pyragius T, Foster BK. Damage and recovery of the bone growth mechanism in young rats following 5-fluorouracil acute chemotherapy. J Cell Biochem. 2006; 99:1688–704. [PubMed: 16888818]
28. Wu X, Chen S, He Y, Rhodes SD, Mohammad KS, Li X, Yang X, Jiang L, Nalepa G, Snider P, Robling AG, Clapp DW, Conway SJ, Guise TA, Yang FC. The haploinsufficient hematopoietic microenvironment is critical to the pathological fracture repair in murine models of neurofibromatosis type 1. PLoS One. 2011; 6:e24917. [PubMed: 21980365]
29. Sharma R, Wu X, Rhodes SD, Chen S, He Y, Yuan J, Li J, Yang X, Li X, Jiang L, Kim ET, Stevenson DA, Viskochil D, Xu M, Yang FC. Hyperactive Ras/MAPK signaling is critical for tibial nonunion fracture in neurofibromin-deficient mice. Hum Mol Genet. 2013; 22:4818–28. [PubMed: 23863460]
30. Weng T, Xie Y, Huang J, Luo F, Yi L, He Q, Chen D, Chen L. Inactivation of Vhl in osteochondral progenitor cells causes high bone mass phenotype and protects against age-related bone loss in adult mice. J Bone Miner Res. 2014; 29:820–9. [PubMed: 23999831]
31. Yokota H, Hamamura K, Chen A, Dodge TR, Tanjung N, Abedinpoor A, Zhang P. Effects of salubrinal on development of osteoclasts and osteoblasts from bone marrow-derived cells. BMC Musculoskelet Disord. 2013; 14:197. [PubMed: 23816340]
32. Broxmeyer HE, Kappes F, Mor-Vaknin N, Legendre M, Kinzfogl J, Cooper S, Hangoc G, Markovitz DM. DEK regulates hematopoietic stem engraftment and progenitor cell proliferation. Stem Cells Dev. 2012; 21:1449–54. [PubMed: 21943234]
33. Mun SH, Won HY, Hernandez P, Aguila HL, Lee SK. Deletion of CD74, a putative MIF receptor, in mice enhances osteoclastogenesis and decreases bone mass. J Bone Miner Res. 2013; 28:948–59. [PubMed: 23044992]
34. Xiao G, Cheng H, Cao H, Chen K, Tu Y, Yu S, Jiao H, Yang S, Im HJ, Chen D, Chen J, Wu C. Critical role of filamin-binding LIM protein 1 (FBLP-1)/migfilin in regulation of bone remodeling. J Biol Chem. 2012; 287:21450–60. [PubMed: 22556421]
35. Rackwitz L, Eden L, Reppenhagen S, Reichert JC, Jakob F, Walles H, Pullig O, Tuan RS, Rudert M, Noth U. Stem cell- and growth factor-based regenerative therapies for avascular necrosis of the femoral head. Stem Cell Res Ther. 2012; 3:7. [PubMed: 22356811]
36. Takahashi S, Fukushima W, Yamamoto T, Iwamoto Y, Kubo T, Sugano N, Hirota Y. Temporal Trends in Characteristics of Newly Diagnosed Nontraumatic Osteonecrosis of the Femoral Head From 1997 to 2011: A Hospital-Based Sentinel Monitoring System in Japan. J Epidemiol. 2015
37. Kim HK, Skelton DN, Quigley EJ. Pathogenesis of metaphyseal radiolucent changes following ischemic necrosis of the capital femoral epiphysis in immature pigs. A preliminary report. J Bone Joint Surg Am. 2004; 86-A:129–35. [PubMed: 14711955]
38. Boss JH, Misselevich I. Osteonecrosis of the femoral head of laboratory animals: the lessons learned from a comparative study of osteonecrosis in man and experimental animals. Vet Pathol. 2003; 40:345–54. [PubMed: 12824505]
39. Hirano T, Majima R, Yoshida G, Iwasaki K. Characteristics of blood vessels feeding the femoral head liable to osteonecrosis in spontaneously hypertensive rats. Calcif Tissue Int. 1996; 58:201–5. [PubMed: 8852577]
40. Masuhara K, Nakata K, Yamasaki S, Miki H, Yoshikawa H. Involvement of platelet activation in experimental osteonecrosis in rabbits. Int J Exp Pathol. 2001; 82:303–8. [PubMed: 11703540]

41. Yun YH, Kim NH, Han DY, Kang ES. An investigation of bone necrosis and healing after cryosurgery, phenol cautery or packing with bone cement of defects in the dog femur. Int Orthop. 1993; 17:176–83. [PubMed: 8340174]

42. Zhang P, Liang Y, Kim H, Yokota H. Evaluation of a pig femoral head osteonecrosis model. J Orthop Surg Res. 2010; 5:15. [PubMed: 20205927]

43. Nishikawa K, Iwamoto Y, Kobayashi Y, Katsuoka F, Kawaguchi S, Tsujita T, Nakamura T, Kato S, Yamamoto M, Takayanagi H, Ishii M. DNA methyltransferase 3a regulates osteoclast differentiation by coupling to an S-adenosylmethionine-producing metabolic pathway. Nat Med. 2015; 21:281–7. [PubMed: 25706873]

44. Zhen G, Wen C, Jia X, Li Y, Crane JL, Mears SC, Askin FB, Frassica FJ, Chang W, Yao J, Carrino JA, Cosgarea A, Artemov D, Chen Q, Zhao Z, Zhou X, Riley L, Sponseller P, Wan M, Lu WW, Cao X. Inhibition of TGF-beta signaling in mesenchymal stem cells of subchondral bone attenuates osteoarthritis. Nat Med. 2013; 19:704–12. [PubMed: 23685840]

45. Cao HJ, Zheng LZ, Wang N, Wang LY, Li Y, Li D, Lai YX, Wang XL, Qin L. Src blockage by siRNA inhibits VEGF-induced vascular hyperpemeability and osteoclast activity - an in vitro mechanism study for preventing destructive repair of osteonecrosis. Bone. 2015; 74:58–68. [PubMed: 25554601]

46. Tower RJ, Campbell GM, Muller M, Gluer CC, Tiwari S. Utilizing time-lapse micro-CT-correlated bisphosphonate binding kinetics and soft tissue-derived input functions to differentiate site-specific changes in bone metabolism in vivo. Bone. 2015; 74:171–81. [PubMed: 25613175]

47. Zhang P, Yokota H. Elbow loading promotes longitudinal bone growth of the ulna and the humerus. J Bone Miner Metab. 2012; 30:31–9. [PubMed: 21748461]

48. Zhang P, Hamamura K, Turner CH, Yokota H. Lengthening of mouse hindlimbs with joint loading. J Bone Miner Metab. 2010; 28:268–75. [PubMed: 19890688]

Highlights

- Knee loading improves bone mass and bone mineral density in osteonecrosis of the femoral head in a rat model.
- Knee loading enhances vessel remodeling through stimulating blood perfusion and angiogenesis.
- Knee loading promotes bone remodeling by suppressing bone-resorbing osteoclasts and increasing bone-forming osteoblasts.
- A significant positive correlation is observed between vessel remodeling and bone healing.

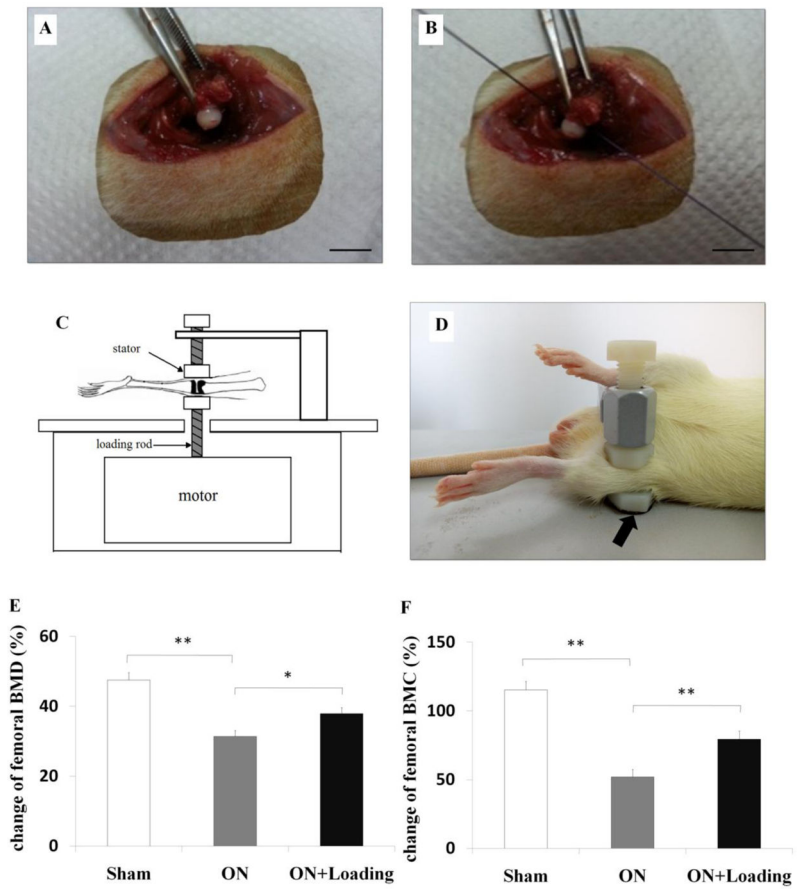

Fig. 1.

The surgical procedure and loading procedure, and the determination of femoral BMD/BMC. (A) The hip joint capsule was transected and the femoral head was dislocated (Bar = 10 mm). (B) ONFH was induced by transecting the ligamentum teres and tightly placing a ligature around the femoral neck (Bar = 10 mm). (C) Schematic diagram illustrated the loading equipment. (D) Loading was laterally applied to the left and right knee of rats successively (5 N at 15 Hz) with 5 min/day for 5 weeks (the loader was indicated by the arrow). (E, F) BMD and BMC of the femur were measured before surgery and sacrifice, and their changes were obtained. Osteonecrosis reduced a regular growth in femoral BMD and BMC. Knee loading increased femoral BMD and BMC. Sham = operated control group, ON = osteonecrosis group, ON+Loading = knee loading treated osteonecrosis group. Asterisks (* and **) represent statistical significance at $p < 0.05$ and $p < 0.01$, respectively (n = 6).

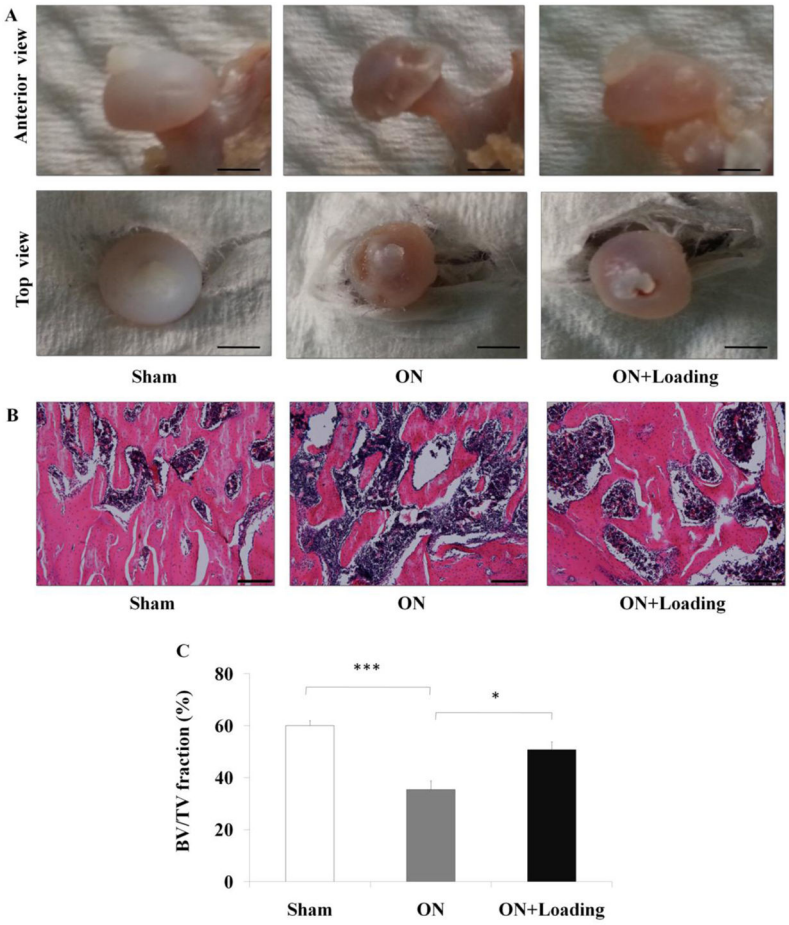

Fig. 2.

The bone healing effect of knee loading on ischemic femoral head. (A) The femoral head surface of the sham group was smooth, and the osteonecrosis group exhibited greater "moth eaten" appearance (indicated by the arrows). The femoral head of the loading group was repaired (Bar = 2 mm). (B) The histological parameters of trabecular in femoral head under the growth plate were determined by H&E staining (100×, Bar = 200 μm). The representative photographs were shown. (C) The osteonecrosis group exhibited a lower ratio of BV/TV. Compared to the osteonecrosis group, knee loading enhanced BV/TV of the femoral head. Asterisks (* and ***) represent statistical significance at $p < 0.05$ and $p < 0.001$, respectively (n = 6).

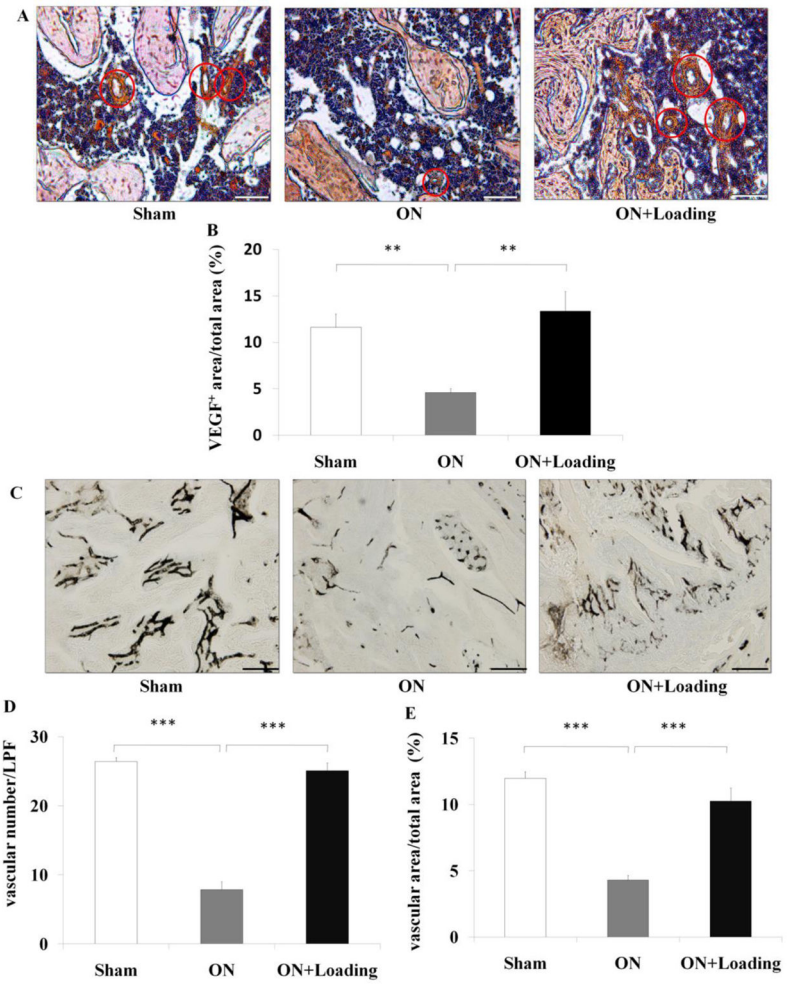

Fig. 3.

Knee loading improved vessel remodeling in the femoral head. (A) The expression of VEGF was measured by immunohistochemistry assay. VEGF positive staining microvessels in femoral head were indicated by the red circles (200×, Bar = 100 μm). (B) The ratio of VEGF positively stained area to total field area was calculated. Osteonecrosis decreased the expression of VEGF, and knee loading enhanced them. (C) The density of microvessels was analyzed in the femoral head using ink blood perfusion angiography (100×, Bar = 200 μm). The representative photographs were shown. (D, E) Osteonecrosis decreased both the vessel number (D) and vessel volume (E), and knee loading significantly enhanced vessel number and volume. Asterisk (** and ***) represent statistical significance at $p < 0.01$ and $p < 0.001$, respectively (n = 6).

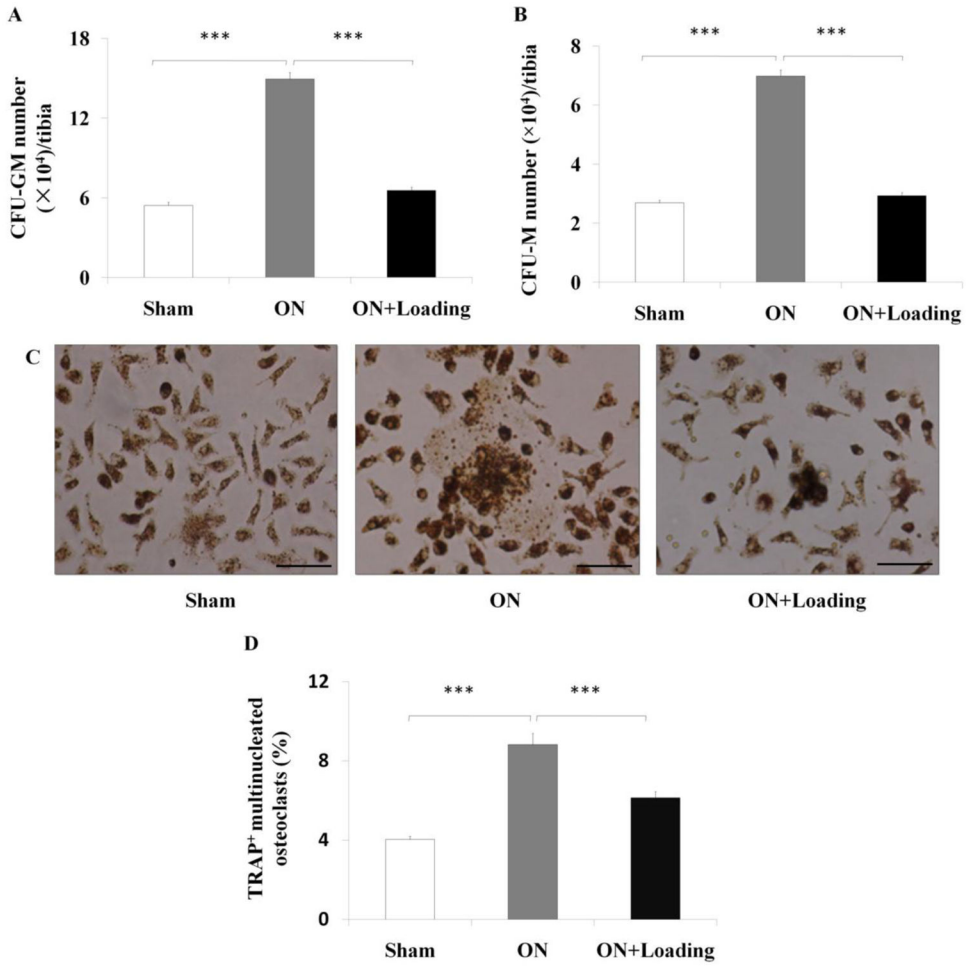

Fig. 4.

Knee loading reduced the numbers of CFU-GM/CFU-M, and suppressed formation of osteoclasts. (A, B) The bone marrow-derived cells were seeded onto 6-well plates at a density of 2.5×10^4 cells/well. The culture medium was composed of methylcellulose with 30 ng/ml M-CSF and 20 ng/ml RANKL. The CFU-GM and CFU-M assays were conducted at day 7. The numbers of CFU-GM and CFU-M per tibia increased in the osteonecrosis group. The numbers of CFU-GM (A) and CFU-M (B) of bone marrow-derived cells were reduced significantly by knee loading. (C) Bone marrow-derived cells were seeded onto 96-well plates at a density of 1×10^5 cells/well. Cells were treated with M-CSF and RANKL for four days. TRAP-positive multinuclear cells (more than 3 nuclei) were identified as osteoclasts, and the ratio of the osteoclast area to the total field area was calculated (400×, Bar = 50 μm). The representative photographs were shown. (D) Cells from the osteonecrosis group exhibited a signicantly increased matured osteoclasts. Knee loading significantly attenuated osteoclast formation. Asterisk (***) represent statistical significance at $p < 0.001$ (n = 6).

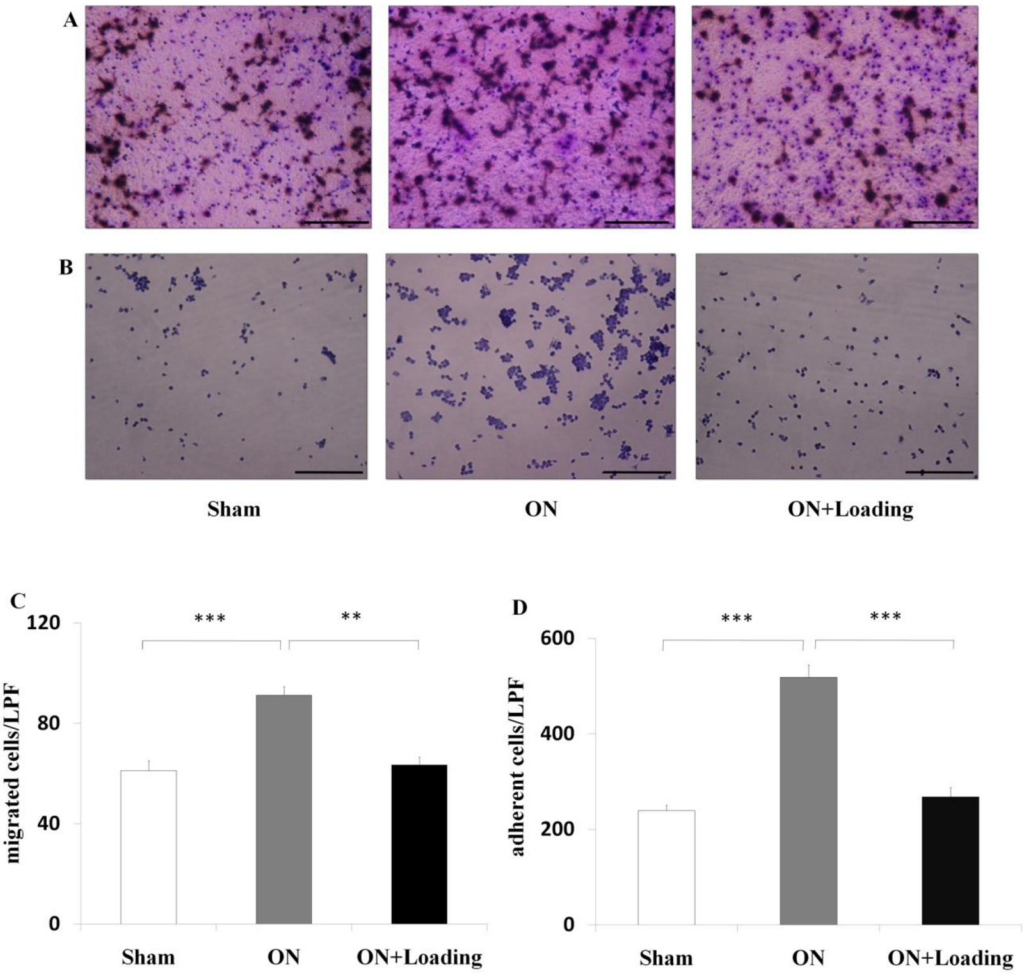

Fig. 5.

Knee loading suppressed migration and adhesion of osteoclasts. (A) Bone marrow-derived cells were treated with M-CSF and RANKL. Then, osteoclast precursors were plated onto vitronectin-coated polycarbonate membrane in 24-well plates at a density of 1×10^5 cells/well at day 4. After 6 h, cells were stained with crystal violet (200×, Bar = 100 μm). The representative photographs were shown. (B) Bone marrow-derived cells were treated with M-CSF and RANKL for two days. Then osteoclast precursors were plated onto vitronectin-coated 96-well plates at a density of 1×10^5 cells/well. After incubation for 1h, adherent cells were stained with crystal violet. The number of cells adherent to the bottom of plates was counted (200×, Bar = 100 μm). The representative photographs were shown. (C) The osteonecrosis group activated osteoclast migration, while knee loading signicantly attenuated osteoclast migration. (D) Cells from the osteonecrosis group exhibited a signicantly increased capacity of osteoclast adhesion. Knee loading significantly reduced osteoclast adhesion. (** and ***) represent statistical significance at $p < 0.01$ and $p < 0.001$, respectively (n = 6).

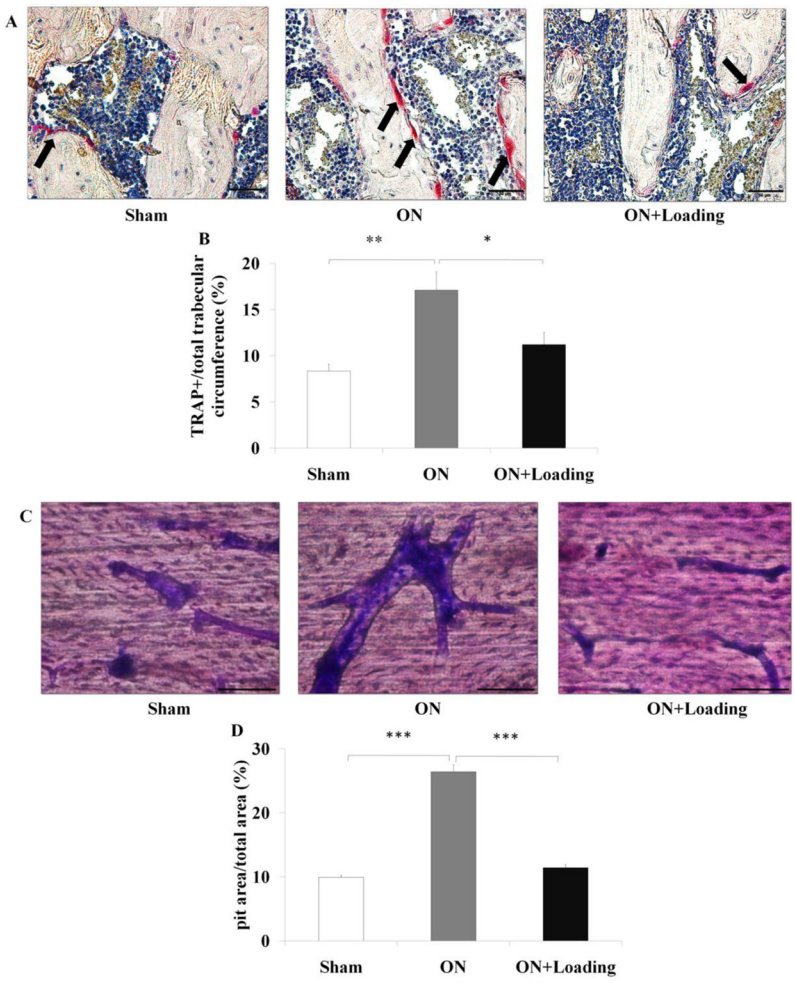

Fig. 6.

Knee loading suppressed bone resorption of osteoclasts. (A) TRAP staining was used to evaluate bone resorption in the femoral head (400×, Bar = 50 μm). TRAP-positive cells, red color, indicated by the arrows. The representative photographs were shown. (B) TRAP staining showed that the ratio of the number of TRAP-positive cells was increased in the osteonecrosis group. The activity of osteoclasts in the osteonecrosis group was significantly suppressed by knee loading. (C) Bone marrow-derived cells were treated with M-CSF and RANKL for 10 days. Then, the bone slices were stained by crystal violet. The ratio of the pit area to the total field area was determined (400×, Bar = 50 μm). The representative photographs were shown. (D) Cells from the osteonecrosis group exhibited a signicantly increased capacity to pits formation. However, bone resorption was suppressed by knee loading. Asterisks (*, ** and ***) represent statistical significance at $p < 0.05$, $p < 0.01$ and $p < 0.001$, respectively (n = 6).

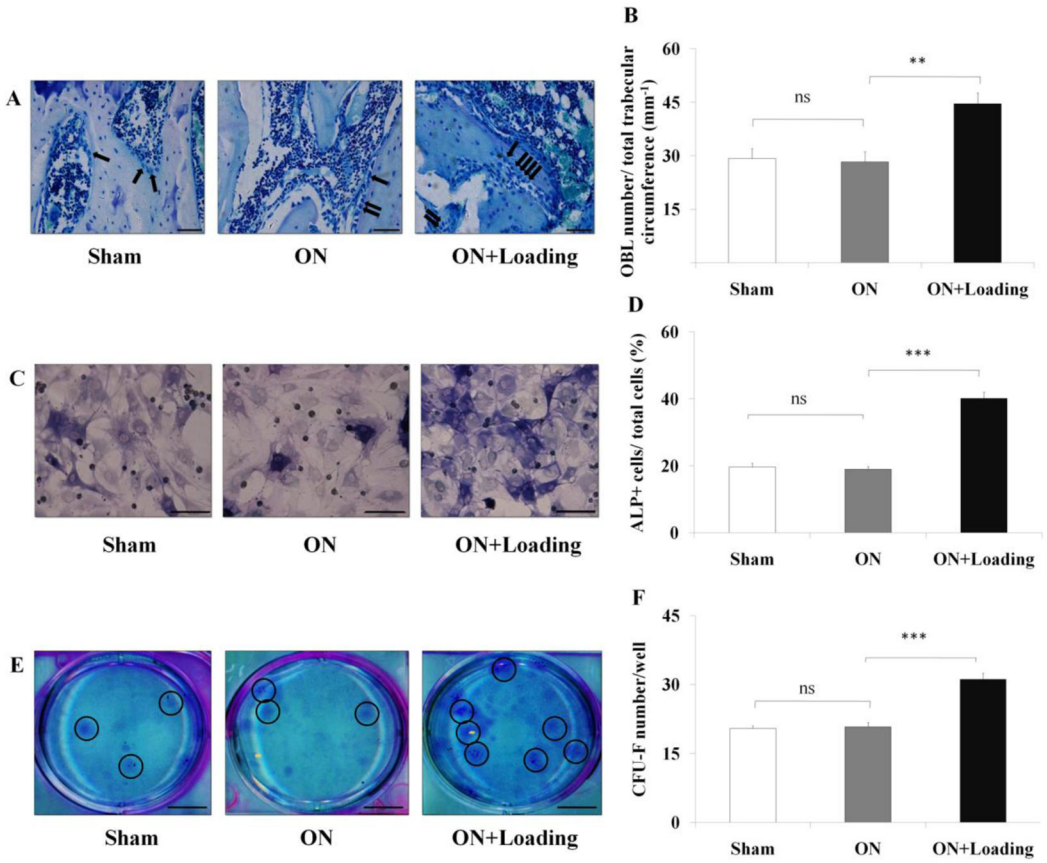

Fig. 7.

Knee loading stimulated differentiation of osteoblast and CFU-F. (A) MacNeal's staining was used to identify osteoblasts in the femoral head (400×, Bar = 50 μm). Osteoblasts, located on trabecular surface, were indicated by the arrows. (B) MacNeal's staining showed that the number of osteoblasts was not significant different in the sham and osteonecrosis groups. However, it signicantly increased in the loading group. (C) Bone marrow-derived cells were cultured in 6-well plates for 14 days. ALP staining was used to detect osteoblast differentiation. The ratio of the numbers of ALP-positive cells to that of total cells was determined (400×, Bar = 50 μm). The representative photographs were shown. (D) The ratio of the number of ALP-positive cells to that of total cells was not significantly different in the sham and osteonecrosis groups. However, this ratio was signicantly increased in the loading group. (E) Bone marrow-derived cells were cultured in 6-well plates with a complete MesenCult medium for 14 days. Fibroblasts were stained using a fibroblast staining kit. The number of colonies per well was counted (Bar = 8 mm). The representative photographs were shown (the clone were indicated by the circles). (F) Cells in the loading group generated a significantly higher number of CFU-F than the sham and osteonecrosis groups. (** and ***) represent statistical significance at $p < 0.01$ and $p < 0.001$, respectively, and ns: $p > 0.05$ (n = 6).

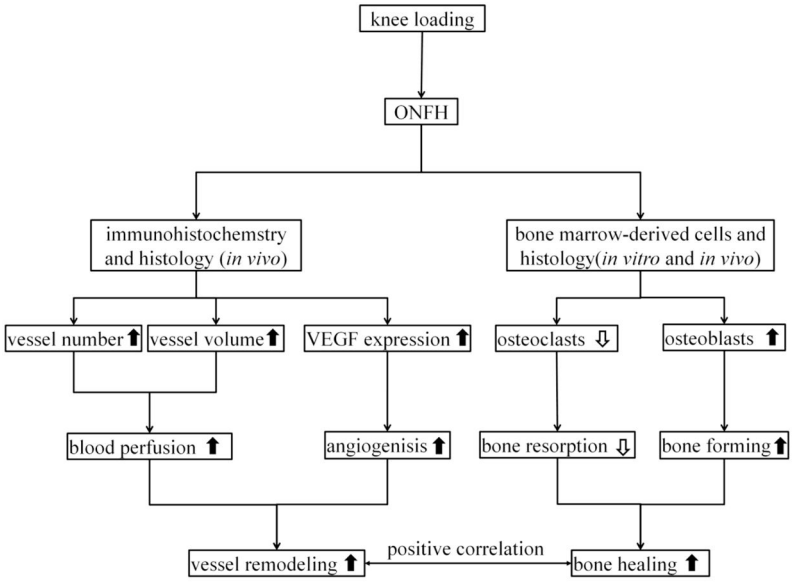

Fig. 8.

Proposed mechanism of knee loading protects against ONFH by enhancing vessel remodeling and bone healing.